Article

Thermal and Structural Analysis of $Mn_{49.3}Ni_{43.7}Sn_{7.0}$ Heusler Alloy Ribbons

Tarek Bachaga [1,2,†], Rakia Daly [2,†], Mohamed Khitouni [2,†], Lluisa Escoda [1,†], Joan Saurina [1,†] and Joan Josep Suñol [1,*]

[1] Department of Physics, University of Girona, Campus Montilivi s/n, Girona 17071, Spain;
E-Mails: lluisa.escoda@udg.edu (L.E.), joan.saurina@udg.edu (J.S.)

[2] Laboratory of Inorganic Chemistry, UR 11ES73, University of Sfax, B.P.1171, Sfax 3000, Tunisia;
E-Mails: bachaga2010@hotmail.fr (T.B.); daly.rakia@gmx.fr (R.D.); khitouni@yahoo.fr (M.K.)

[†] These authors contributed equally to this work.

[*] Author to whom correspondence should be addressed; E-Mail: joanjosep.sunyol@udg.edu;
Tel.: +34-972-419-757; Fax: +34-972-418-098.

Academic Editor: Kevin H. Knuth

Abstract: The martensitic transformation and the solidification structures of $Mn_{49.3}Ni_{43.7}Sn_{7.0}$ alloy ribbons prepared by melt-spinning were investigated by means of scanning electron microscopy, X-ray diffraction and differential scanning calorimetry. In those experiments special attention was given to melt spinning processing parameters such as the linear surface speed of the copper wheel rotating, the injection overpressure and the distance between wheel and injection quartz tube. Transformation entropy was found higher when increasing linear surface speed or the distance from injection point to wheel. The resulting samples showed chemical compositions close to the nominal ones and, at room temperature, crystallized in a monoclinic single-phase martensite with 14M modulation (without a significant variation in the cell parameters). Strong dependence of ribbon thickness on processing parameters was found. The average grain size varied between 1.6 and 6.6 μm, while the start temperature of the martensitic temperature varied from 394 to 430 K.

Keywords: entropy; enthalpy; X-ray diffraction; magnetic shape memory

PACS Codes: 65.40gd; 61.66Dk

1. Introduction

Rapid solidification offers advantages over conventional metallurgy processes to develop alloys with specific functional properties following the increasing demand for high performance materials [1–3]. A refined microstructure, structural and chemical homogeneity and extension of solid solubility are some of the unique features achieved through rapid solidification [4,5]. Normally, cooling rates of 10^6–10^8 K/s are employed in this process, which are values much higher than the cooling rates applied for conventional solidification processes, *i.e.*, rates of 10^2 K/s or less. Therefore, the rapid solidification of alloys by the melt-spinning process can lead to better mechanical properties compared to those obtainable by conventional casting [5]. In the case of Heusler-based ferromagnetic Ni-Mn-X (X = Sn, In, Ga, Sb) alloys, many attempts have been made to produce rapidly solidified forms. That is due to their extensive applications in the magnetic refrigeration, aerospace, and automotive industries [6]. In particular, these alloys have the ability to undergo a reversible first-order martensitic transformation (FOMT) from a high-temperature cubic austenite phase to a structurally martensite phase [7,8]. FOMT takes place by the diffusionless shearing of the parent austenitic phase. By lowering the temperature, a cubic high temperature parent austenite phase transforms into a tetragonal, orthorhombic, or monoclinic martensite, depending on the composition and manufacturing conditions. Likewise, martensite can be also modulated (10M or 14M). The complex behavior exhibited by non-stoichiometric Ni-Mn-Sn Heusler alloys is due to the strong coupling between magnetism and structure. These alloy systems form an interesting class of materials because of the reported large magnetocaloric effect due to their high entropy [9]. A specific feature of these alloys is that the saturation magnetization is greatly reduced (or becomes almost zero) for temperatures over the structural transformation point from austenite to martensite [10,11]. Recently, some interesting reports on the physical properties of Mn-Ni-Sn Heusler alloy have been published. Coll *et al.* [12] found that Mn-Ni-Sn alloys are fully single-phase with a cubic structure austenite phase at room temperature and this thermally transforms into structurally modulated orthorhombic martensite upon cooling. Martensitic transformation in rapidly solidified $Mn_{50}Ni_{40}In_{10}$ alloy ribbons was first reported by Sanchez *et al.* [13]. For technological application it is important to develop alloys with the martensitic transformation temperatures around a desired temperature, for instance room temperature. It is also necessary to improve their entropy values for applications such as magnetic refrigeration. On the other hand, extensive research, including computer modeling, have propelled the understanding of martensite; the average grain size of a polycrystalline shape memory alloy have been correlated with martensitic transformation temperature M_s [14–16]. In other works this correlation is less considered, *i.e.*, in the case of Ni-Mn-X alloys (X = Sn, In, Sb), three factors to which M_s has been mainly related were reported: the number per unit volume of nucleation-related defects characteristic, the probability of nucleation of the martensite phase in the austenite matrix and that the chemical free energy overcome the free energy to initiate the crystalline transformation [14–16]. Rapid solidification techniques such as melt-spinning are effective for obtaining single-phase alloy ribbons in the $Ni_{50}Mn_{50-x}Sn_x$ system [17,18]. Mn-rich alloys of the Mn-Ni-(In/Sn) system hold the promise for higher saturation magnetization owing to their higher Mn content [19].

On the other hand, no detailed information about the effects of the solidification parameters on the thermodynamics (entropy, enthalpy) and microstructure (crystalline structure, grain size) in the melt-spun $Mn_{49.3}Ni_{43.7}Sn_{7.0}$ alloys are available in the present literature. Therefore, ribbons of the same

$Mn_{49.3}Ni_{43.7}Sn_{7.0}$ composition were produced under different melt spinning conditions in order to check the influence on their entropy and characteristic transformation temperatures. We also have analyzed the microstructure of the ribbons, and for these purposes, scanning electron microscopy (SEM), X-ray diffraction (XRD) and differential scanning calorimetry (DSC) investigations have been carried out on the ribbons produced by melt-spinning.

2. Experimental procedure

Polycrystalline Mn-Ni-Sn alloy ingot was prepared by arc melting high purity (99.99%) elements under an argon environment in a water-cooled copper crucible. The ingot was melted three times to ensure a good homogeneity. Next, the ingot was melt-spun on a rotating copper wheel set at different processing parameters: linear wheel speed (30 or 48 ms^{-1}), injection overpressure (900 or 400 mbar) and distance between wheel and injection quartz crucible (1.5 or 3 mm). The as-spun ribbon samples obtained under different parameters were labelled R1 (30 m/s, 400 mbar, 3 mm), R2 (48 m/s, 400 mbar, 3 mm), R3 (48 m/s, 400 mbar, 1.5 mm) and R4 (48 m/s, 900 mbar, 3 mm), respectively.

Thermal and structural analyses were performed by applying several techniques. Scanning electron microscopy (SEM) investigations were carried using a DSM 960A microscope operating at 30 kV and linked with an energy dispersive X-ray spectrometry (EDX) device (Carl Zeiss, Oberkochen, Germany). X-ray diffraction (XRD) analyses were performed at room temperature with a D500 X-ray powder diffractometer using Cu-K$_\alpha$ radiation (Siemens, Berlin and Munich, Germany). The structure of samples is refined by applying Jana software (Jana 2006, Jana, Praha, Czech Republic) [20]. Thermal analyses were performed by differential scanning calorimetry (DSC) using a DSC830 calorimeter (Mettler Toledo, Greifensee, Switzerland) with a heating/cooling rate of 10K/min under argon atmosphere in a temperature range of 350–600 K.

3. Results and Discussion

SEM micrographs showed differences in the thickness and grain size, which seem to be influenced by the processing parameters. Figure 1 shows the SEM micrographs of the free surface and fracture morphology (insets) of the various $Mn_{49.3}Ni_{43.7}Sn_{7.0}$ ribbons: (a) R1, (b) R2, (c) R3 and (d) R4. Table 1 also lists the chemical compositions obtained by EDX measurements. From EDX analysis, the average composition of the four alloys is $Mn_{49.3}Ni_{43.7}Sn_{7.0}$. The standard deviation obtained for the elemental chemical composition (as determined by EDX) was 0.4–0.6 at% for Ni, 0.4–0.6 at% for Mn, and 0.3–0.5 at% for Sn. One parameter used to characterize magnetic shape memory alloys is the electron-to-atom ratio (e/a) that is calculated using the electron concentration of the outer shells for each element of the Ni-Mn-Sn alloy. The number of electrons per atom (e/a ratio) for Ni, Mn, Sn atoms are $10(3d^8, 4s^2)$, $7(3d^5, 4s^2)$ and $4(5s^2, 5p^2)$. The following expression is used to calculate e/a ratios as described in detail in [14]:

$$e/a = (10 \times \text{at}\%Ni + 7 \times \text{at}\%Mn + 4 \times \text{at}\%Sn)/100 \tag{1}$$
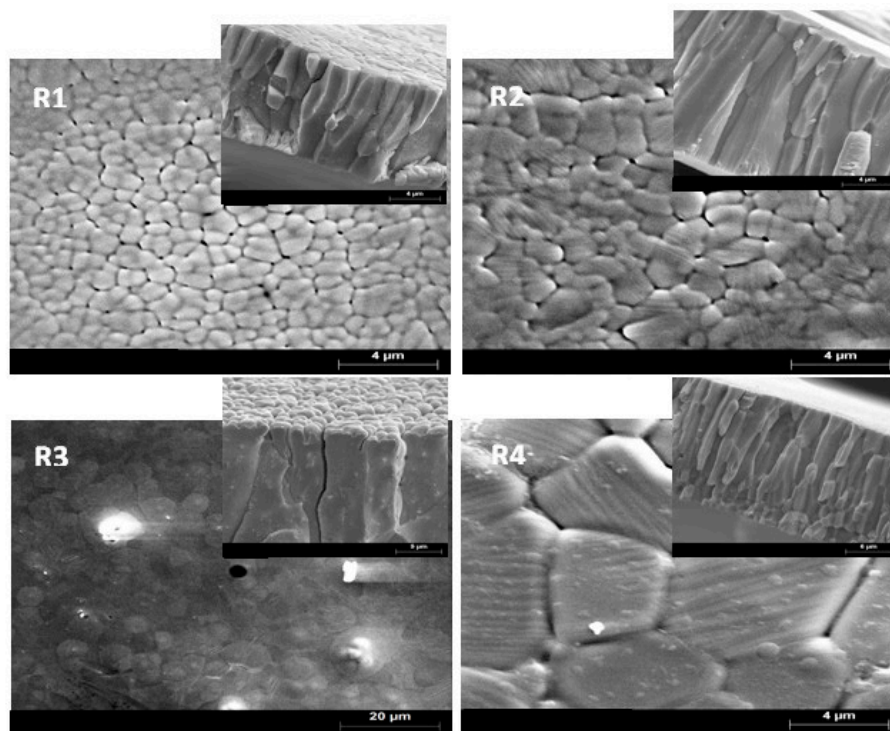
Figure 1. SEM micrographs showing the surface microstructure of ribbons on the free surface and fractured cross section (insets).

The calculated average grain size <d> in the free surface for heat-treated ribbons is also listed in Table 1. It can be noted that the effect of rapid solidification on the thickness and grain size varies with the different parameters used. For R1 and R2, the main difference between the samples is the linear speed on the wheel surface. Although usually the particle size has no significant dependence on cooling rate [21,22], the cooling rate is so high that the grain growth kinetics are limited by the rate of crystallization. The increasing of the wheel surface speed from 30 to 48 ms^{-1} results in the decrease of the ribbon thickness from 15.5 to 10 µm. These results are in reasonable agreement with those obtained by Tkatch *et al.* [23]. For ribbon R3, small equiaxed grains were found to crystallize in a thin layer on the wheel side. In addition, columnar grains growth along the solidification axis. The grains are as large as the thickness of the strip allows. The highest thickness was found in samples R3 and R4. The longer axis of the columnar grains tends to be aligned perpendicularly to the planar tape surface.

Table 1. Ni, Mn and Sn atomic concentration, e/a parameter, thickness and average grain size <d> for samples R1, R2, R3 and R4.

Sample	Mn (at%)	Ni (at%)	Sn (at%)	e/a	<d> (µm)	Thickness (µm)
R1	49.1	43.9	7.0	8.11	1.7	15.5
R2	49.4	43.5	7.1	8.09	1.6	10
R3	49.4	43.7	6.9	8.10	5.5	20
R4	49.1	44.0	6.9	8.11	6.6	19

Figures 2 (samples R1 and R2) and 3 (samples R3 and R4) show the room temperature XRD patterns. All the diffraction patterns were successfully indexed and identified with the monoclinic structure using Rietveld analysis via the Jana software. All the alloys were single-phase (*i.e.*, there were no secondary phases detected). The structure of the samples was of nearly the same pattern except for small differences in the peak intensities and angles. These results are consistent with electron microscopy observations of the martensitic structure.
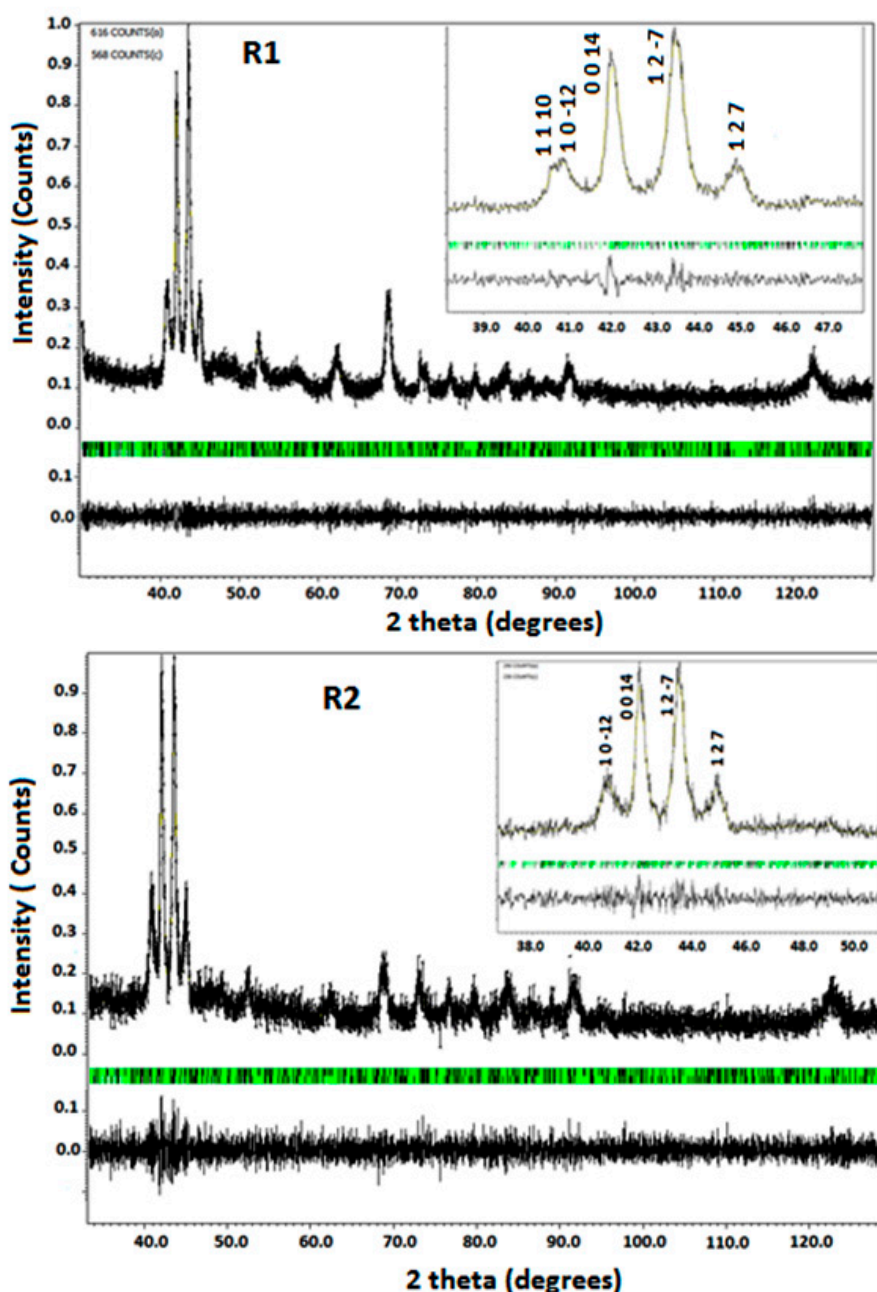
Figure 2. Rietveld graphical output of the structural refinement of the modulated martensite phase (samples R1 and R2). The black and green ticks specify the main reflections and satellites, respectively. The inset shows the selected areas in a range of 2θ values.
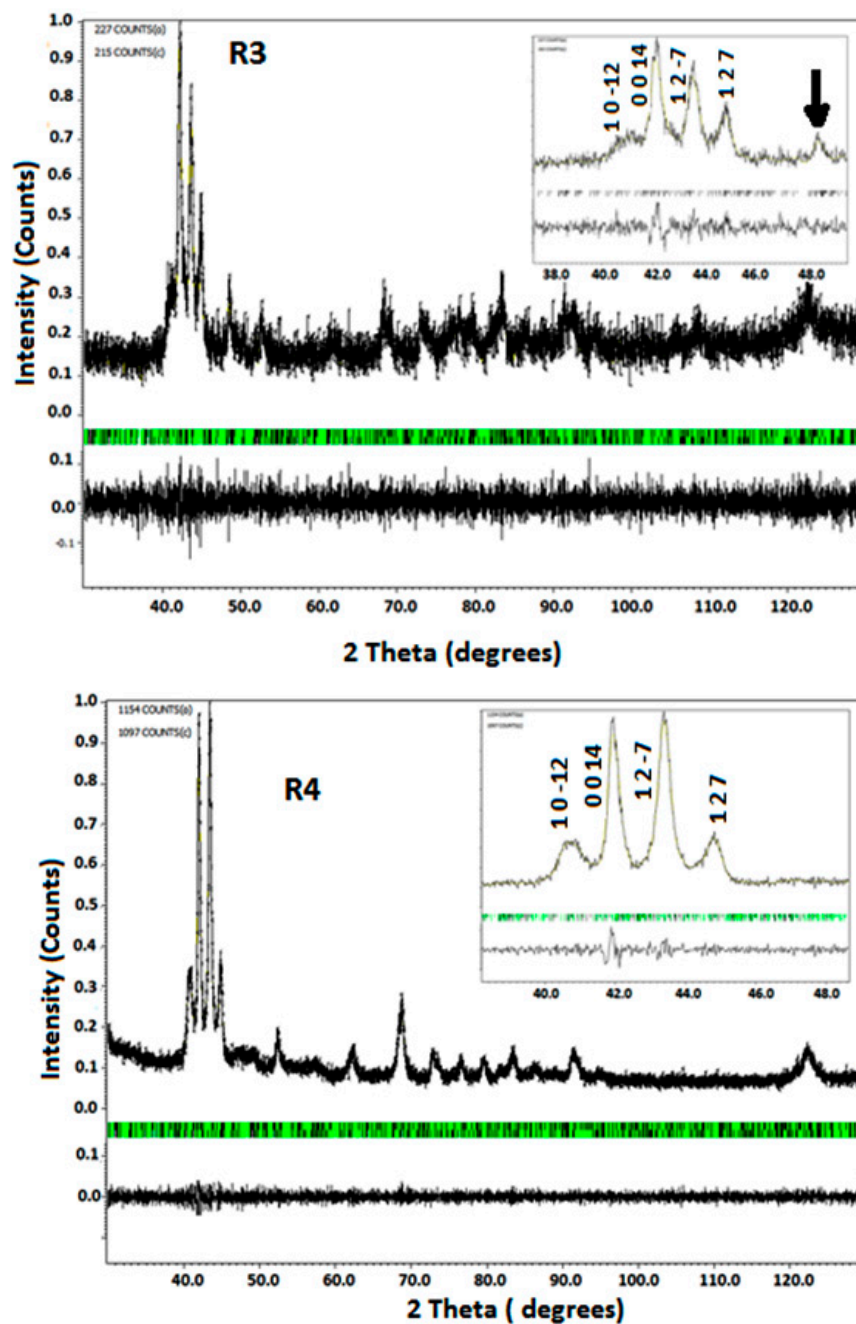
Figure 3. Rietveld graphical output of the structural refinement of the modulated martensite phase (samples R3 and R4). The black and green ticks specify the main reflections and satellites respectively. The inset shows the selected areas in a range of 2θ values. The arrow indicates the bump corresponding to 2θ position of the second-order satellite with respect to the 0 0 14 main reflection.

The lattice parameter for samples R1, R2, R3, and R4 are listed in Table 2. These parameters are in good agreement with those previously reported for melt-spun ribbons of close chemical composition [9,10]. In our work, the differences in the lattice parameters and volume between samples are small (e.g., <1%). suggesting that the possible change in M_s is not linked to the change of Mn-Mn interatomic distance. The fitting parameter R_p values are 0.0918, 0.127, 0.0815 and 0.09 for samples R1, R2, R3 and R4 respectively. The diffraction peaks are broad probably due to: (a) crystallographic defects

and (b) inhomogeneity of the samples. It is known that annealing favors both: (a) improvement of the homogeneity and (b) diminution of crystallographic defects. Furthermore, the difference of the peaks intensity is due to anisotropy and texture effects favored by the columnar grains microstructure of the ribbons.

Table 2. Crystallographic parameters and cell volume of $Mn_{49.3}Ni_{43.7}Sn_{7.0}$ alloys.

Sample	Crystallography parameters					Volume (nm³)
	a (nm)	b (nm)	c (nm)	β(°)	q	
R1	0.43077(2)	0.56003(3)	29.961(2)	93.65	0.4226	0.10308 (2)
R2	0.43012(3)	0.56109(4)	29.389(2)	93.55	0.4222	0.10315 (1)
R3	0.43405(3)	0.55785(3)	30.022(3)	93.85	0.4220	0.10343 (2)
R4	0.43011(3)	0.55935(2)	29.987(3)	93.53	0.4120	0.10249 (2)

The Rietveld analyses (Figures 2 and 3) show additional peaks alongside the main reflections indicating the presence of structural modulation and the structural distortion due to modulation is considered incommensurate. Nevertheless, the values of the modulation vector q are close to commensurate ratio 3/7 (0.42857). Thus, only short atomic displacements from commensurate modulation were found. The main difference with 3/7 is obtained in sample produced by increasing the injection overpressure (R4). This sample has also the lower volume.

Figures 4 and 5 show the DSC heating and cooling curves of $Mn_{49.3}Ni_{43.7}Sn_{7.0}$ melt-spun alloy ribbons. The characteristic transformation temperatures at which martensite start and finish (M_s and M_f) and austenite start and finish (A_s and A_f) are collected in Table 3. The hysteresis is due to the increase of the elastic and surface energies during the martensite formation. Thus, the nucleation of the martensite implies supercooling. The transformation region can be also characterized by the martensite transformation temperature T_0: the temperature at which the Gibbs energies of the martensitic and parent phases are equal.
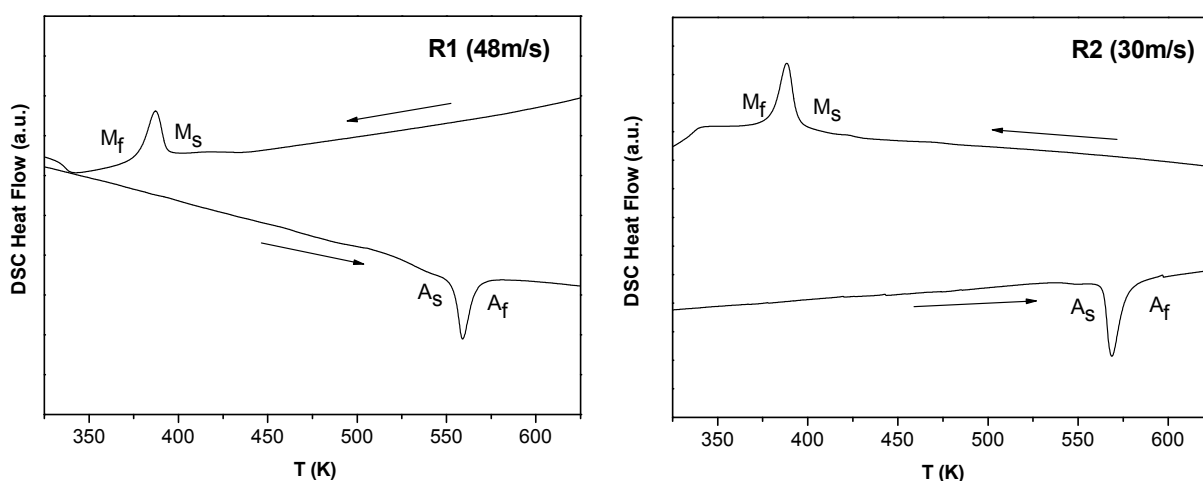
Figure 4. DSC scans (heating and cooling) of samples R1 (up) and R2 (down).
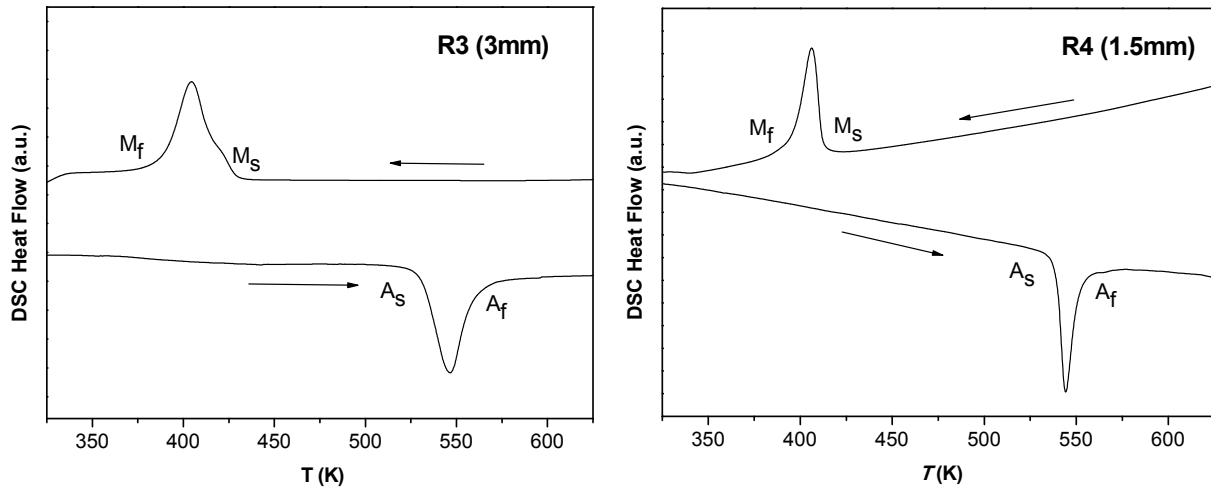
Figure 5. DSC scans (heating and cooling) of samples R3 (up) and R4 (down).

The thermodynamic equilibrium condition is: $\Delta G = 0 = \Delta H - T_0\Delta S$. It follows that $T_0 = \Delta H/\Delta S$. Thus, T_0 increases (decreases) if ΔH increases (decreases) and/or ΔS decreases (increases):

$$T_o = \frac{1}{2}(M_s + A_f) \tag{2}$$

T_o values are 490 K, 482 K. 483 K and 499 K for alloys R1, R2, R3 and R4 respectively.

Usually the heat exchange, Q, of the transformation determined as the area of the DSC peak is defined as the enthalpy change, ΔH, of the transformation. Thus, the entropy (ΔS) and enthalpy (ΔH) changes in the structural transformations are calculated from calorimetry data using the relationships:

$$\Delta H = \int_{T_i}^{T_t}\left[\left(\frac{dQ}{dt}\right)\left(\frac{dT}{dt}\right)^{-1}\right]dT \tag{3}$$

and:

$$\Delta S = \int_{T_i}^{T_t}\left[\frac{1}{T}\left(\frac{dQ}{dt}\right)\left(\frac{dT}{dt}\right)^{-1}\right]dT \tag{4}$$

where T_i and T_f are the temperature limits of integration.

Nevertheless, recent works take into account that heat exchange, Q, during the transformation process is not exactly equal to the change in enthalpy, ΔH, of the transformation [24]. The difference between Q and ΔH is determined by the contribution of: (a) the elastic energy E_{el} and (b) the irreversibly dissipated energy W_d:

$$Q = \int_{Ms/As}^{Mf/Af} T(dS) = (\Delta H - E_{el} + W_d) \tag{5}$$

One approach to determine both parameters (E_{el} and W_d) is to establish their relation with the characteristic temperatures of the reversible transformation. For practical purposes, a good estimation of both terms can be made in accordance with reference [24]:

$$E_{el} = \frac{1}{4}\times[\Delta S\times[(A_f - A_s) + (M_s - M_f)]] \tag{6}$$

and:

$$W_d = \frac{1}{2} \times [\ \Delta S \times (A_f + A_s) + (M_s + M_f)\ ] \tag{7}$$

Transformation temperatures (A_s, A_f, M_s, M_f) and heat exchange are determined from DSC scans. From Equations (5)–(7) the following four parameters are unknown: ΔH, ΔS, E_{el} and W_d. By combining previous equations with the thermodynamic equilibrium conditions it is possible to determine the relative fraction of E_{el} and W_d from the enthalpy of the transformation: $E_{el}/\Delta H$ and $W_d/\Delta H$. For ΔH we use the average between cooling and heating data.

It is found that the characteristic transformation temperatures are very sensitive to the production conditions. For example, the ribbon produced with the lowest linear wheel speed (R1) has also the lowest values of the E_{el} and W_d terms. In addition, by increasing the wheel linear speed, both values increase. Thus, the melt spinning processing parameters influence more the microstructure (grain size) and the transformation temperatures than the crystallographic structure.

The e/a ratio is also considered a factor that affects the start temperature of the martensitic transformation, M_s [12,13]. Nevertheless, EDX results given in Table 1 indicate that the e/a parameter does not change significantly. However, at this stage we must also consider that EDX allows the determination of the elemental chemical composition with an accuracy of 0.1 at% and how this uncertainty modifies the resulting M_s value. Assuming a difference in the Mn (or Ni) content of ±0.1 at% and given the nearly linear (e/a) dependence of the M_s temperature given in [6]. We obtained that M_s only varies by ±2 K. Thus, changes in thermal behavior are probably controlled by small microstructural changes due to different processing conditions. It is known that the atomic order of the austenitic parent phase influences the transformation temperatures. For example, the disorder between Mn and Ga atoms in Ni_2MnGa alloy diminishes M_s about 100 K [25]. Likewise annealing favors microstructural changes as the transition from B2 to $L2_1$ or the improvement of the chemical homogeneity of the alloy. Furthermore, with proper annealing the temperature range of transformation is narrower [26].

Table 3 shows than the fraction of ΔH that remains in the system as elastic energy is smaller (<4.4%) that the fraction of ΔH associated to dissipated energy (between 26.5% and 36.3%). It is not found a general relation between both values and the transformation characteristic temperatures. Similar values for the entropy are obtained in samples R2, R3 and R4 whereas the value is lower in sample R1. This effect can be explained by the fact that this sample was produced with the lowest wheel speed. This effect reduces the temporal relative amount of material in contact with the wheel during first stage of solidification and the subsequent high heat transfer needed for rapid solidification. High entropy and low dissipated fraction are found in samples R3 and R4, whereas the highest elastic energy fraction corresponds to sample R4 (the highest injection overpressure). It is obvious that the thermodynamic parameters can be modified by altering melt spinning conditions. Nevertheless, a thermodynamic approach is not enough to explain the sample behavior. From the microstructural point of view, the main conclusion is that small grains have a stabilizing effect in the austenitic phase increasing thermal hysteresis, probably because they limit the volume of the individual martensite variants [15,24]. Consequently, in our work it was found that thermal hysteresis is lower/higher in samples with higher/lower grain size and thickness (R3 and R4 / R1 and R2). It was also reported [18] a relation between the density of dislocations, ρ, and the diameter of the martensitic grain: $\rho = 1\ /\ <d>$.

Thus, the control of the production conditions is necessary to modify both the microstructure and the thermal behavior (transformation temperatures and entropy).

Table 3. Transformation temperatures and thermodynamic parameters: h and c indicates data obtained by heating or cooling DSC scans respectively.

Sample	R1	R2	R3	R4
A_s (K)	564	548	538	528
A_f (K)	584	570	552	568
M_s (K)	396	394	414	430
M_f (K)	376	374	388	384
T_0 (K)	490	482	483	499
Q (J g^{-1})	11.97 (h) 12.909 (c)	15.741 (h) 14.463 (c)	14.582 (h) 15.873 (c)	16.601 (h) 16.876 (c)
ΔH (J g^{-1})	16.563 (h) 17.224 (c)	20.406 (h) 20.284 (c)	19.203 (h) 19.649 (c)	20.807 (h) 21.152 (c)
ΔS (J g^{-1} K^{-1})	0.0317 (h) 0.0352 (c)	0.042 (h) 0.041 (c)	0.0394 (h) 0.0408 (c)	0.0416 (h) 0.0423(c)
$E_{el}/\Delta H$ (%)	1.74	2.17	2.17	4.31
$W_d/\Delta H$ (%)	26.5	36.3	29.8	28.3

4. Conclusions

Melt-spun ribbons of Mn$_{49.3}$Ni$_{43.7}$Sn$_{7.0}$ composition were produced by rapid solidification using the melt-spinning technique by applying different process conditions. The microstructure shows the existence of equiaxial and columnar grains with an inhomogeneous distribution, whereas the chemical composition is homogeneous. The average grain size varies between 1.6 and 6.6 µm. The reduction in the average grain size is accompanied by a decrease in the start temperature of the martensitic transformation, M_s demonstrating that the structural transition temperatures can be tuned within certain limits by controlling this microstructural parameter. Furthermore, it is found that the transformation entropy is lower in alloy produced at lower linear surface speed, probably due to the reduction of the temporal relative amount of material in contact with the wheel during first stage of solidification. Minor entropy differences have been found between samples with different values of the injection overpressure or the distance between wheel and injection point. Likewise, from EDX and XRD analysis ribbons have nearly constant elemental chemical composition and monoclinic cell parameters for modulated martensite (14M) structure at room temperature. The modulation vector, q, values are close to those of commensurate modulation 3/7 indicating low atomic displacement from commensurate sites. The highest displacement is found in the sample produced at the lowest linear wheel speed.

Acknowledgments

Author Contributions

T. Bachaga is a doctorate student. The thesis works are supervised by J.J. Suñol and M. Khitouni. M.L. Escoda supports EDX and SEM analysis. J. Saurina DSC analysis and Rakia Daly XRD analysis. All authors have read and approved the final manuscript.

Conflicts of Interest

The authors declare no conflict of interest.

References and Notes

1. Jones, H. A perspective of the development of rapid solidification and nonequilibrium processing and its future. *Mater. Sci. Eng. A* **2001**, *304*, 11–19.
2. Hong, S.J.; Suryanarayana, C.; Chun, B.S. Section-dependent microstructure and mechanical properties of rapidly solidified and extruded Al-20Si alloy. *Mater. Res. Bull.* **2004**, *39*, 465–474.
3. Sánchez, T.; Bonastre, J.; Santos, J.D.; Sánchez, M.L.; Chizhik, A.; González, J.; Suñol, J.J.; Hernando, B. The effect of field quenching fabrication on the magnetoimpedance response in $Co_{66}Fe_4Ni_1Si_{15}B_{14}$ amorphous ribbons. *J. Appl. Phys.* **2012**, *111*, doi:10.1063/1.3687417.
4. Lavernia, E.J.; Ayers, J.S.; Sritvasan, T.S. Rapid solidification processing with specific application to aluminium alloys. *Int. Mater. Rev.* **1992**, *37*, 1–44.
5. Anantharman, T.R.; Suryanarayana, C. *Rapidly Solidified Metals: A Technological Overview*; Trans Tech Publications: Pfaffikon, Switzerland, 1987.
6. Krenke, T.; Acet, M.; Wassermann, E.F.; Moya, X.; Mañosa, L.;Planes, A. Martensitic transitions and the nature of ferromagnetism in the austenitic and martensitic states of Ni-Mn-Sn alloys. *Phys. Rev. B* **2005**, *72*, doi:10.1103/PhysRevB.72.014412.
7. Planes, A.; Mañosa, L.; Acet, M. Magnetocaloric effect and its relation to shape-memory properties in ferromagnetic Heusler alloys. *J. Phys. Cond. Matter* **2009**, *21*, doi:10.1088/0953-8984/21/23/233201.
8. Cong, D.Y.; Roth, S., Potschke, M.; Hurrich, C.; Schultz, L. Phase diagram and composition optimization for magnetic shape memory effect in Ni-Co-Mn-Sn alloys. *Appl. Phys. Lett.* **2010**, *97*, doi:10.1063/1.3454239.
9. Krenke, T.; Duman, E.; Acet, M.; Wassermann, E.F.; Moya X.; Mañosa, L.; Planes, A. Inverse magnetocaloric effect in ferromagnetic Ni-Mn-Sn alloys. *Nat. Mater.* **2005**, *4*, 450–454.
10. Krenke, T.; Acet, M.; Wassermann, E.F.; Moya, X.; Mañosa, L.; Planes, A. Ferromagnetism in the austenitic and martensitic states of Ni-Mn-Sn alloys. *Phys. Rev. B* **2006**, *73*, doi:10.1103/PhysRevB.72.174413.
11. Khovaylo, V.V.; Skokov, K.P.; Gutfleisch, O.; Miki, H.; Takagi, T.; Kanomata, T.; Koledov, V.V.; Shavrov, V.G.; Wang, G.; Palacios, E.; *et al.* Pecularities of the magnetocaloric properties in Ni-Mn-Sn ferromagnetic shape memory alloys. *Phys. Rev. B* **2010**, *81*, doi: 10.1103/PhysRevB.81.214406.
12. Coll, R.; Escoda, L.; Saurina, J. Sánchez-Llamazares, J.L.; Hernando, B.; Suñol, J.J. Martensitic transformation in Mn-Ni-Sn Heusler alloys. *J. Therm. Anal. Calorim.* **2010**, *99*, 905–909.

13. Sánchez-Llamazares, J.L.; Sánchez, T.; Santos, J.D.; Pérez, M.J.; Hernando, B.; Escoda, L.; Suñol, J.J.; Varga, R. Martensitic phase transformation in rapidly solidified $Mn_{50}Ni_{40}In_{10}$ alloy ribbons. *Appl. Phys. Lett.* **2008**, *92*, doi:10.1063/1.2827179.

14. Hirth, J.P. Influence of grain-boundaries on mechanical properties. *Metal. Trans.* **1972**, *3*, 3047–3067.

15. Guimaraes, J.R.; Rios, P.R. Unified description of martensite microstructure and kinetics. *J. Mater. Sci.* **2009**, *44*, 998–1005.

16. Seki, K.; Kura, H.; Sato, T.; Taniyama, T. Size dependence of martensite transformation temperature in ferromagnetic shape memory alloy FePd. *J. Appl. Phys.* **2008**, *103*, doi:10.1063/1.2890143.

17. Santos, J.D.; Sánchez, T.; Álvarez, P.; Sánchez, M.L.; Sánchez-Llamazares, J.L.; Hernando, B.; Escoda, L.; Suñol, J.J.; Varga, R. Microstructure and magnetic properties of $Ni_{50}Mn_{37}Sn_{13}$ Heusler alloy ribbons. *J. Appl. Phys.* **2008**, *103*, doi:10.1063/1.2832330.

18. Xuan, H.C.; Xie, K.X.; Wang, D.H.; Han, Z.D.; Zhang, C.L.; Cu, B.X.; Du, Y.W. Effect of annealing on the martensitic transformation and magnetocaloric effect in $Ni_{44.1}Mn_{44.2}Sn_{11.7}$ ribbons. *Appl. Phys. Lett.* **2008**, *92*, doi:10.1063/1.2948904.

19. Wu, Z.; Liu, Z.; Yang, H.; Liu, Y.; Vu, G. Metamagnetic phase transformation in $Mn_{50}Ni_{37}In_{10}Co$ polycrystalline alloy. *App. Phys. Lett.* **2011**, *98*, doi: 10.1063/1.3554423.

20. Petrisek, V.; Dusek, M. Jana2000: The crystallographic computing system. Institute of Physics: Prague, Czech Republic. Available online: http://www.xrey.fzu.cz/jana/jana.html (accessed on 1 February 2014).

21. Zayak, A.T.; Adeagbo, W.A.; Entel, P.; Rabe, K.M. e/a dependence of the lattice instability of cubic Heusler alloys from first principles. *Appl. Phys. Lett.* **2006**, *88*, doi:10.1063/1.2185046.

22. Zheng, H.X.; Wu, D.Z.; Xue, S.C.; Frenzel, J.; Eggeler, G.; Zhai, Q.J. Martensitic transformation in rapidly dolidified Heusler $Ni_{49}Mn_{39}Sn_{12}$ ribbons. *Acta Mater.* **2011**, *59*, 5692–5699.

23. Tkatch, V.; Limanovskii, A.I.; Demisenko, S.N.; Rassolov, S.G. The effect of the melt spinning of processing parameters on the rate cooling. *Mater. Sci. Eng. A* **2002**, *323*, 91–96

24. Quintana-Nedelcos, A.; Sánchez-Llamazares, J.L.; Rios-Jara, D.; Lara-Rodríguez, A.G.; García-Fernández, T. Effect of the quenching rate on the average grain size and martensitic transformation temperature in rapidly solidified polycrystalline $Ni_{50}Mn_{37}Sn_{13}$ alloy ribbons. *Phys. Stat. Sol. A* **2013**, *210*, 2159–2165.

25. Shamberger, P.J.; Ohuchi, F.S. Hysteresis of the martensitic phase transition in magnetocaloric effect of Ni-Mn-Sn alloys. *Phys. Rev. B* **2009**, *79*, doi:10.1103/PhysRevB.79.144407.

26. Kreissl, M.; Neumann, K.U.; Stephens, T.; Ziebeck, K.R.A. The influence of atomic order on the magnetic and structural properties of the ferromagnetic shape memory compound Ni_2MnGa. *J. Phys. Cond. Matter* **2003**, *15*, 3831–3839.

27. Besseghini, S.; Pasquale, M.; Passaretti, F.; Sciacca, A.; Villa, E. NiMnGa polycrystalline magnetically activated shape memory alloy: Calorimetric investigation. *Scr. Mater.* **2001**, *44*, 2681–2687.